



Blank Frame and Intensity Variation Distortion Detection and Restoration Pipeline for Phase-Contrast Microscopy Time-Lapse Images

Mahmut Ucar¹, Leonardo O. IHEME², Sevgi Onal³, Devrim Pesen-Okvur⁴, Ozden Yalcin-Ozuyisal⁴, Behcet U. Toreyin⁵, Devrim Unay¹

¹Department of Electrical and Electronics Engineering, Faculty of Engineering, Izmir Democracy University, Izmir, Turkey

²Virasoft Inc, New York, USA

³Department of Biotechnology and Bioengineering, Izmir Institute of Technology Graduate School of Science and Engineering, Izmir, Turkey

⁴Department of Molecular Biology and Genetics, Izmir Institute of Technology Faculty of Science, Izmir, Turkey

⁵Department of Artificial Intelligence and Data Engineering, Istanbul Technical University Informatics Institute, Istanbul, Turkey

Cite this article as: M. Ucar, et al. "Blank frame and intensity variation distortion detection and restoration pipeline for phase-contrast microscopy time-lapse images," *Electrica*, 24(1), 60-66, 2024.

ABSTRACT

In this study, we propose a preprocessing pipeline for the detection and correction of distorted frames in time-lapse images obtained from phase-contrast microscopy. The proposed pipeline employs the average intensities of frames as a foundational element for the analysis. In order to evaluate the degree of correction required for intensity variance, a normalization technique is applied to the difference between the average intensity of a specific frame and the median average intensity of all frames within the study. Our restoration method increases the histogram similarity between the distorted and non-distorted frames, preserves trans-passing pixels in regions of interest, and mitigates the development of additional distortions. The efficacy of the proposed method was evaluated using 15 395 time-lapse image frames from 27 experiments using our own dataset and 830 time-lapse images from four different experiments obtained from the cell tracking challenge. The results of the validation demonstrate a high degree of numerical and visual accuracy of the proposed pipeline.

Index Terms— Blank frame, intensity variation, phase-contrast microscopy, preprocessing, restoration, video processing.

This work is supported by the Scientific and Technological Research Council of Turkey (TUBITAK) under grant no 119E578. The data used in this study is collected under the Marie Curie IRG grant (no: FP7 PIRG08-GA-2010-27697).

Corresponding author:

Devrim Unay

E-mail:

unaydevrim@gmail.com

Received: March 16, 2023

Revision Requested: May 2, 2023

Accepted: July 14, 2023

Publication Date: January 8, 2024

DOI: 10.5152/electrica.2024.23030



Content of this journal is licensed under a Creative Commons Attribution-NonCommercial 4.0 International License.

I. INTRODUCTION

For many studies, data preprocessing is a crucial step. Data preprocessing has been demonstrated to be vital for the success of proposed techniques in both deep-learning-based solutions and traditional machine learning-based solutions [1–4]. The popularity of phase-contrast microscopy (PCM) and its applications has increased significantly in recent years [5–10]. To achieve high success rates in downstream pipelines, a preprocessing pipeline that incorporates correction for different distortions is necessary.

Histogram equalization (HE) and adaptive HE (AHE) are often used for image enhancement in phase-contrast microscopy images (PCMI). However, PCMI does not use the full gray-level intensity range available, so applying HE or AHE to non-distorted frames can result in significant changes. In comparison, contrast-limited adaptive HE (CLAHE) is a more suitable approach for PCMI data [11]. Contrast-limited adaptive HE displays blood vessels more clearly than HE and AHE, but it also generates more noise. As a result, median filtering is used as a postprocessing step after CLAHE.

A de-flickering technique was proposed by [12], but it requires high frame-rate videos as input, whereas the videos in our data collection (in audio video interleave format with 20 fps) consist of frames acquired every 15 minutes. The proposed approach of [12] further differs from ours in that it utilizes local intensity change, but in our data, intensity variations affect the entire frame.

Other methods for intensity correction have also been proposed for magnetic resonance [13–16], ultrasound [17], and infrared [18] images. However, these methods underperform when applied to PCMI data. For example, [13] suggested a physical correction method for intensity nonuniformity in magnetic resonance images, while [14–16] presented computational

methods for magnetic resonance imaging (MRI) intensity inhomogeneity correction. On ultrasound B-mode images, a segmentation approach with inhomogeneous intensity correction was also proposed by [17].

While contiguous z-stacked grayscale images are a typical feature of MRIs, ultrasound images, and PCMIs, the suggested approaches were built on the nonuniformity of the intensity distribution. For both distorted and undistorted frames, PCMI mostly has a uniform intensity separation in the background; there is very little change in pixel intensities, and for non-distorted frames, all pixels are on a small percentage of the separation interval. Furthermore, we are looking for a global (whole frame) intensity correction as compared to the local intensity correction that the physical correction method proposed.

Similarly, as proposed in [18], nonuniformity correction is a frequent image-enhancement process used to compensate for infrared detector drifts caused by changes in the scene or surroundings. In comparison to our proposed median thresholding procedure, the weighted average of neighboring frames method used in [18] requires more computation. Our goal is not to obtain the best fit with the following frames, because the best-fitting histogram may cause new noises, as discussed in Section III.

In this paper, we present a novel pipeline that takes a video (PCM time-lapse images) as input, generates appropriate quality-related metrics, and corrects any detected distorted frames. The pipeline currently detects and restores blank frames as well as frames with intensity variation.

The paper is organized as follows: The PCM data used are described in Section II, the proposed detection and restoration solutions for blank frame and intensity variation distortions are introduced in Section III, the results of our proposed solutions are reported in Section IV, and the findings are summarized in Section V.

II. DATA

The dataset used in this study was provided by the Molecular Biology and Genetics Department at the Izmir Institute of Technology. It comprises 27 PCM cell motility assays, with a focus on detecting and correcting two specific types of distortions: blank frames and intensity variations. Visual examples of these distortions can be found in the links of references [19] and reference [20]. In addition to our dataset, the proposed algorithm was also evaluated on the cell tracking challenge dataset [21–23], which contains 830 non-distorted frames.

Ground truth classifications for both datasets were provided by experts through two different methods: 1) video-level classification, which involved watching a video and categorizing it according to the type of distortion present and 2) frame-level classification, where each frame of a video was visually analyzed using ImageJ software [24] categorized according to the type of distortion observed. It should be noted that in frame-level ground truth classification, monotonically decreasing intensity distortion, which is also observed in our dataset, was not considered as it can be attributed to the nature of the experiments.

III. METHODS

We focus on the detection and restoration of blank frames and intensity variations, which are commonly observed in Z-PCM images.

These distortions present challenges for cell-tracking algorithms, as blank frames may result in the loss of cell trajectories, and intensity variations can lead to the extraction of inconsistent or unrepresentative features for segmentation algorithms. Our restoration approach is based on the assumption that the pixel intensity distribution of a given frame follows a half-normal distribution [25] and that the distribution does not have a long tail.

The proposed method is outlined in the flowcharts shown in Fig. 1. The flow starts with reading the video format of PCM time-series images. Then, the calculation of average frame intensity (AFI) is started and when the last frame is calculated, the calculation of AFI has been completed. The AFI values will be used for both blank frame and intensity variation distortion detection and reconstruction parts of the algorithm. Because of that reason, AFI values have been saved into a vector. In blank frame detection, AFI vector values are floored, and if they reach zero, related frames are flagged as blank frames. The intensity variation detection and reconstruction algorithm follows the blank frame detection part. The first frame is recalled from the video and the AFI values of the related frame are compared with α times the median value of the floored AFI vector. Selecting the suitable α value is explained in the following paragraphs. If the difference between current and α times median AFI values is not coherent with distortion, the related frame will be written into a new video and then continue with the next frame. If the next frame is flagged as blank frame distortion, the related frame is just skipped, and if the difference of current and α times median AFI values is coherent with intensity variation distortion, the reconstruction algorithm will be triggered. The standard deviation of AFI values will be calculated, and the result will be normalized by dividing by 255, which shows the error percentage between related frames. The current frame's every pixel will be rearranged with that error percentage. Pixel intensities will either increase or decrease, depending on whether the related frame is getting darker or brighter. The reconstructed frame is written into the new video with respect to related order, and the algorithm calls the following frame until the last frame is read. Then, the generation of the new video is completed as the output of the algorithm.

Blank frames in our dataset are a result of laboratory data collection errors and/or intentionally inserted for the purpose of analysis. Regardless of the cause of blank frames in videos, they negatively impact downstream processes such as cell segmentation and cell tracking. In some videos, the intensity between neighboring frames abruptly changes. The origin of this distortion is uncertain, but experts agree that it is the result of unintentional changes in the brightness of the light source. The pseudo code of the proposed blank frame detection algorithm is given in Fig. 2. In a nutshell, the AFI is calculated for every frame. Then, its floored version is thresholded using a fixed value of 0. Frames satisfying this thresholding (i.e., = 0) are flagged as blank frames.

Acceptable error percentage of intensity variation is denoted by α in Fig. 1. To determine a suitable value for this parameter α , five videos from our data collection were studied, and an experimentally optimal value of 0.3 was selected. Accordingly, fluctuations in intensity that are higher than 30% of the average intensity of the adjacent frames are flagged. The restoration algorithm is performed after the detection algorithm, using both the video and the results of the detection as inputs. The pseudo code of the proposed intensity variation detection and restoration algorithm is given in Fig. 3. Simply, to detect frames with intensity variation, each frame's AFI is compared

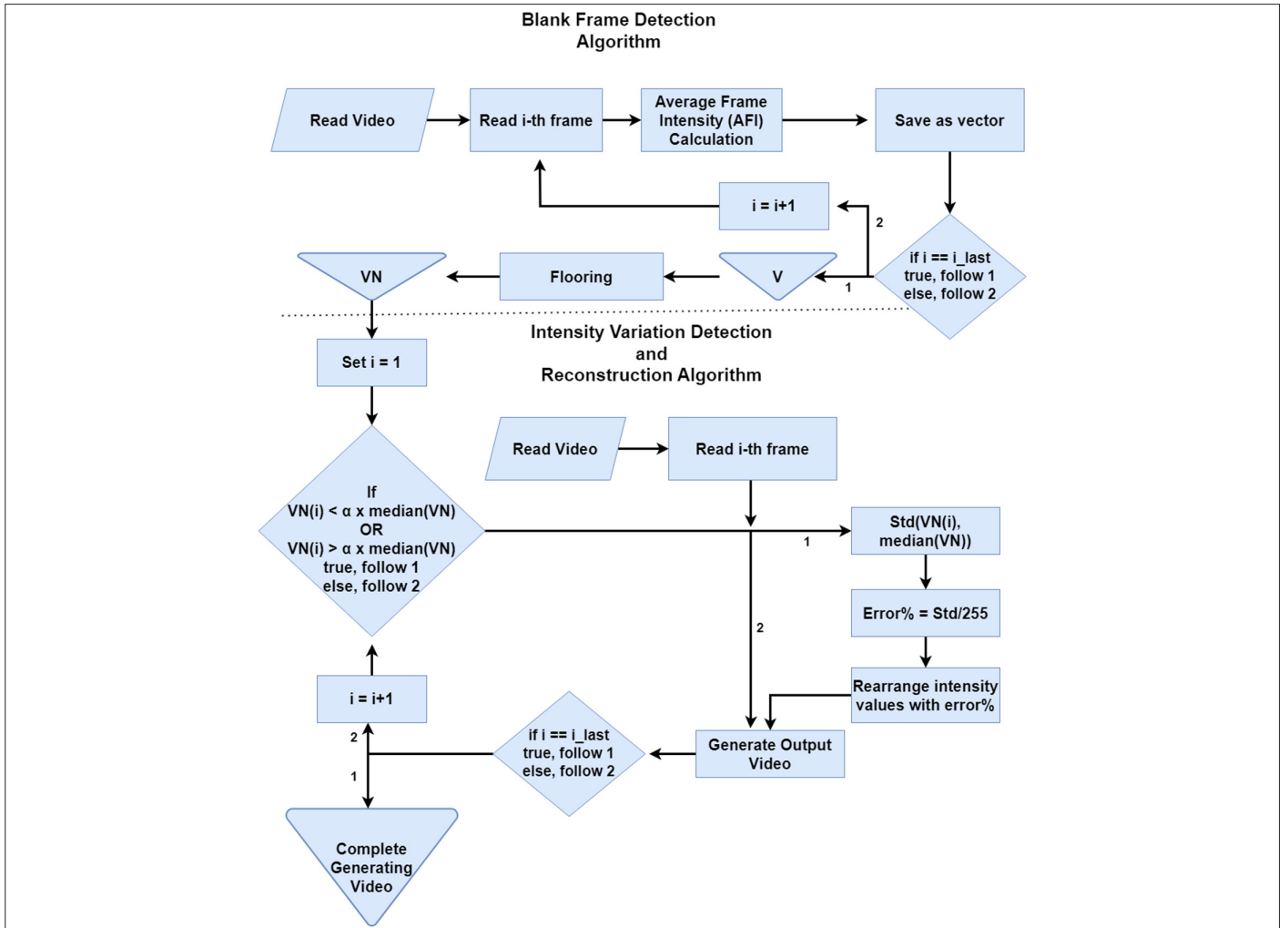


Fig. 1. Flowcharts of our proposed blank frame detection and intensity variation correction algorithms. Here, AFI stands for average frame intensity, α represents acceptable error percentage, VN is for nonblank vector, std() is standard deviation, and median() is for median operator.

```

INPUT Video
INPUT VN
INPUT V

SET i to 1
REPEAT
    std(i) is equal to (V(i) - median(V))
    INCREMENT i
UNTIL to the last element of V

READ video
SET pos to 1
REPEAT
    INCREMENT i
    READ frame
    IF VN(i) is not 1 (not blank screen)
        IF V(i) larger or smaller than alpha times of median(V)
            K is equal to floored value of every pixel of "frame x std(i)/100"
            L is equal to, "frame + (ones x std(i)/100)"
            L is median of K and L
            write M into NewVideo
        ELSE
            write frame into NewVideo
    END IF
END IF
UNTIL to the last frame of video
OUTPUT NewVideo
    
```

Fig. 2. Pseudo code for the blank frame detection algorithm.

```

INPUT Video
INPUT VN
INPUT V

SET i to 1
REPEAT
    std(i) is equal to (V(i) - median(V))
    INCREMENT i
UNTIL to the last element of V

READ video
SET pos to 1
REPEAT
    INCREMENT i
    READ frame
    IF VN(i) is not 1 (not blank screen)
        IF V(i) larger or smaller than alpha times of median(V)
            K is equal to floored value of every pixel of "frame x std(i)/100"
            L is equal to, "frame + (ones x std(i)/100)"
            L is median of K and L
            write M into NewVideo
        ELSE
            write frame into NewVideo
    END IF
END IF
UNTIL to the last frame of video
OUTPUT NewVideo
    
```

Fig. 3. Pseudo code for intensity variation detection and restoration algorithm

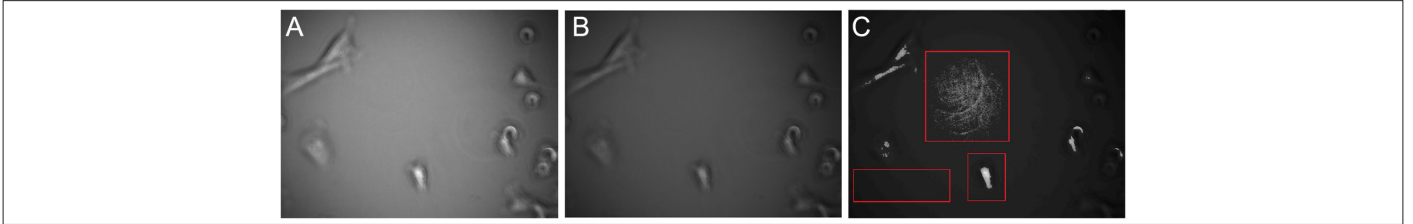


Fig. 4. (a) A distorted frame, (b) output of the proposed intensity restoration algorithm applied on the distorted frame, and (c) output of the conventional histogram matching (HM) applied on the distorted frame. Structural similarity metric between (a) and closest non-distorted frame is 0.49 and between (b) and closest non-distorted frame is 0.85. Red boxes represent the distortions the HM algorithm caused, namely salt noise at the center of the frame, very high intensities at the center of cells, and regional intensity changes.

against $a \times \text{median}$ (AFI vector) and flagged as frames with lower or higher intensities accordingly. Here, the AFI vector corresponds to the AFI values across the whole video. Finally, reconstruction in the flagged frames is realized by adjusting their intensities with the standard deviation of the normalized AFI vector. An exemplary result can be seen in Fig. 4 where the distorted frame (Fig. 4-a) is reconstructed using traditional histogram matching technique (Fig. 4-b) and the proposed algorithm (Fig. 4-c).

Phase-contrast microscopy image histograms typically occupy only a small portion of the 8-bit intensity range. When an intensity variation occurs, the histogram distribution tends to cover a broader spectrum. A histogram matching (HM) technique was used to test the hypothesis that it is possible to restore distorted frames using the histograms of non-distorted frames. The distorted frame and the frame that returned the median value of the AFI vector were the inputs to the HM method. However, as shown in Fig. 4-c, the HM algorithm also caused the following distortions: salt noise at the center of the frame, very high intensities at the center of cells, and regional intensity changes.

We have developed a new approach to address the limitations of the HM method. Our approach 1) preserves regional intensity changes, 2) does not introduce additional noise, and 3) generates a histogram that closely resembles the non-distorted frame. We calculate the normalized standard deviation (σ^n) of the distorted frame and express the difference between the median AFI and the average intensity for the current frame as σ^n . To make the algorithm more robust to changes, we chose to use the median value of the AFI of frames rather than the mean value. The restored frame is generated using (1) by adjusting each pixel at a specific rate while still preserving the regional trans-passing information of the PCMI.

$$K = [I \times (1 - \sigma^n)] \quad (1)$$

where I is an $n \times m$ intensity matrix, σ^n is the normalized standard deviation, and K is the output of (1).

In our analysis, we employed (1) as a means of reconstructing the frames of the image sequence under consideration. However, it was observed that the output presented a significant reduction in pixel intensities. In order to address this issue, we modified the equation to become (2). This modification ensured that the regional trans-passing pixels were retained while simultaneously reducing the pixel intensities by a specific rate.

Furthermore, in order to further enhance the quality of the reconstructed frames, we employed (3), which arithmetically modifies

the pixel intensities. The final step in our reconstruction process involved calculating the final equation, (4), by taking the median of the resulting frames from (2) and (3). The output generated by this final equation is illustrated in Fig. 4-b and demonstrates the effectiveness of our proposed method in improving the quality of the reconstructed frames.

$$L = I \frac{\sigma_i^n}{100} \quad (2)$$

$$M = I + J \times \frac{\sigma_i^n}{100} \quad (3)$$

$$R = \frac{L + M}{2} \quad (4)$$

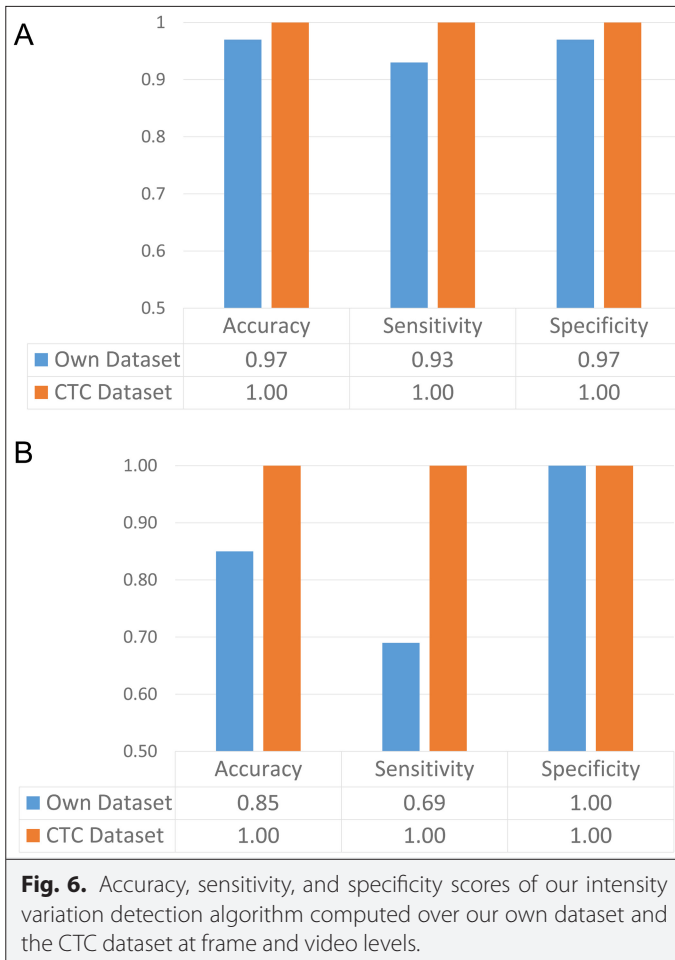
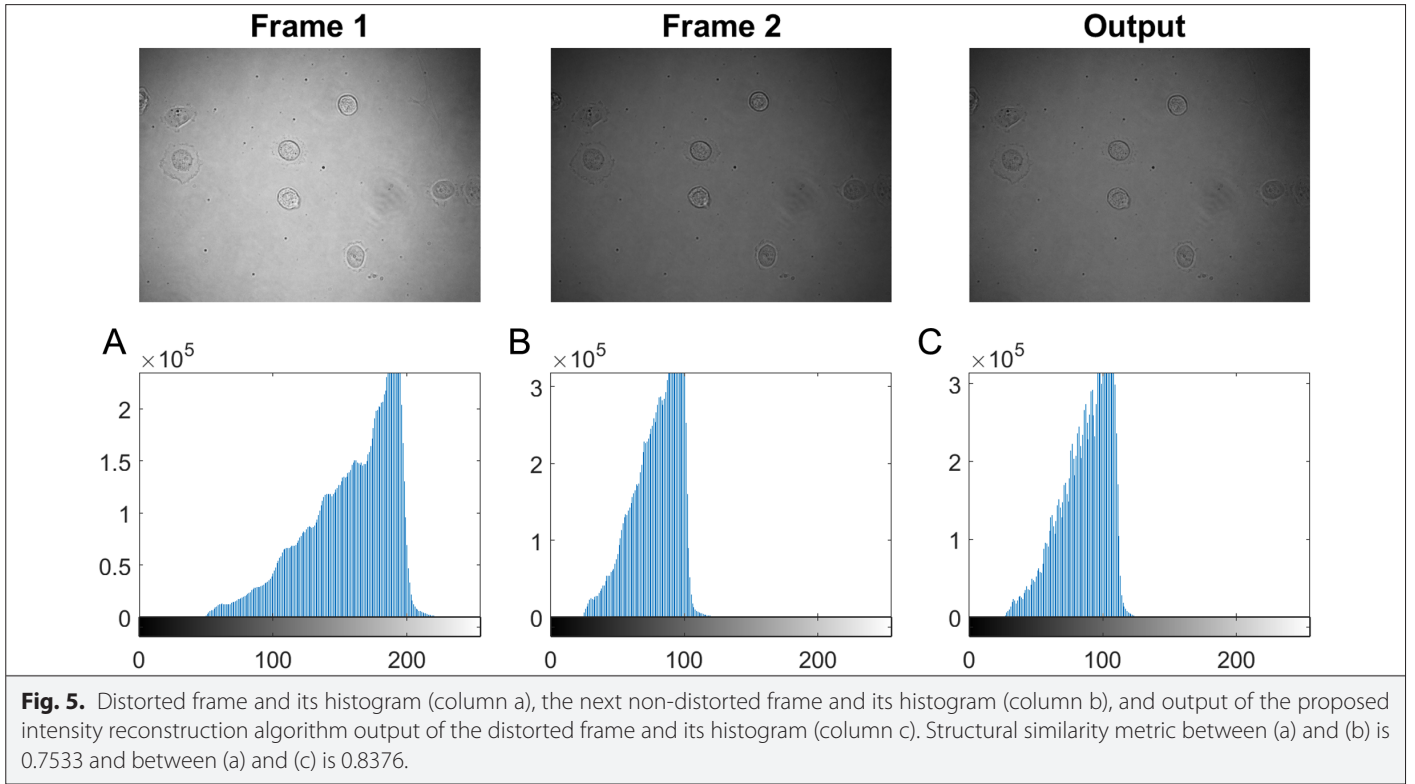
where $\hat{\sigma}_i^n$ refers to the i 'th element of the normalized standard deviation, J is a matrix of ones with the same size as I , L is the output of (2), M is the output of (3), and R is the output of (4) which is the reconstructed frame.

Fig. 5 displays a sample distorted frame, its reconstructed version which was generated using our suggested technique, and a subsequent non-distorted frame together with the relevant histograms. As shown, the histogram of the distorted frame covers a wider region of the 8-bit spectrum than the histogram of the non-distorted frame.

We used traditional performance metrics to evaluate the effectiveness of our proposed algorithms in detecting distortions. These metrics include true positive (TP), false positive (FP), true negative (TN), and false negative (FN), as well as the accuracy ($\frac{TP + TN}{TP + TN + FP + FN}$), sensitivity ($\frac{TP}{TP + FN}$), and specificity ($\frac{TN}{TN + FP}$) scores derived from them. In this context, a TP indicates a correctly detected distorted frame, and a TN refers to a correctly detected non-distorted frame. The performance of the algorithms was evaluated both on a frame-by-frame basis, considering each individual frame, and on a video-by-video basis, where a video was labeled as non-distorted if it did not contain any distorted frames.

IV. RESULTS

In the PCM dataset provided in Section II, we evaluated the effectiveness of our detection methods for blank frame and intensity variation distortions at both the frame and video levels. The performance of our method for detecting blank frames achieved perfect scores of "1" for accuracy, sensitivity, and specificity. This indicates that our method correctly detects every blank frame without any false alarms



for both our own dataset and the CTC: Cell Tracking Challenge dataset. It is important to note that the PCM dataset is unbalanced, with only 164 of the 15 395 frames having blank frame distortion and 446 having intensity variation distortion, resulting in an overall distorted frame rate of 0.04%. Despite this imbalance, the proposed approach demonstrates robustness.

In terms of intensity variation reconstruction, our proposed algorithm generates more visually pleasing results than the traditional HM technique Fig. 4. The accuracy, sensitivity, and specificity values for the detection of intensity variations at both the video and frame levels are shown in Fig. 6 for both our own dataset and the CTC dataset. As seen in Table I, the algorithm achieves highly accurate video level detection with only 4 FNs. As mentioned in Section II, monotonic intensity variation videos were not labeled at the frame level, and it should be noted that 386 FPs (Table I) belong to such videos.

Overall, our proposed technique effectively restores intensity variations by providing a histogram that mimics that of the following

TABLE I. VIDEO AND FRAME-LEVEL CONFUSION MATRICES OF OUR PROPOSED INTENSITY VARIATION DETECTION ALGORITHM FOR OUR DATASET AND CTC DATASET SEPARATELY

		TP	FP	TN	FN
Our dataset	Video-level detection	9	0	14	4
	Frame-level detection	413	386	14 538	31
CTC dataset	Video-level detection	0	0	4	0
	Frame-level detection	0	0	830	0

FN, false negative; FP, false positive; TN, true negative; TP, true positive.

non-distorted frame without introducing further distortions such as rapid local intensity changes or noise. As can be seen in Fig. 5, the histogram of the distorted frame mimics (in this case, becomes narrower) that of the following non-distorted frame. Additionally, our proposed algorithm achieved higher structural similarity values between reconstructed and closest non-distorted frames compared to distorted and closest non-distorted frames. For the image shown in Fig. 4, the structural similarity metric value increased from 0.4890 to 0.8539, and for the images shown in Fig. 5, the structural similarity metric value increased from 0.7533 to 0.8376. The state-of-the-art methods, HE, AHE, and CLAHE applied to the frame shown in Fig. 5. The structural similarity metric values had calculated between the reconstructed and next non-distorted frame. The results are as follows: HE=0.6009, AHE=0.5673, and CLAHE=0.3447. The proposed algorithm achieved a better reconstruction with a higher similarity.

V. CONCLUSION

In this study, we presented a novel preprocessing pipeline for the detection and restoration of distorted frames in PCM time-lapse images. Our focus was on two types of distortions, blank frames and intensity variations across frames, which can negatively impact the efficiency of segmentation and tracking algorithms. By evaluating our proposed methods on PCM time-lapse images from 27 cell motility videos of our own dataset and four CTC experiments, we demonstrated exceptional performance in the detection of blank frames and extremely high accuracy in the detection of intensity variations. While blank-frame distortions can be corrected by simply excluding them from the video stream, frames with intensity variations must be restored in a lossless manner. To achieve this, our proposed restoration algorithm accurately balances the average intensities between frames without distorting in-frame information. Future studies can expand our pipeline to include the detection and restoration of geometric and optical deformations.

Peer-review: Externally peer-reviewed.

Author Contributions: Concept – D.P.O., O.Y.O., D.U.; Design – L.O.I., D.P.O.; Supervision – L.O.I., D.P.O., B.U.T., D.U.; Funding – D.P.O., O.Y.O., B.U.T., D.U.; Materials, Data Collection and/or Processing – M.U., S.O., O.Y.O.; Analysis and/or Interpretation – M.U., L.O.I., D.U.; Literature Review – M.U.; Writing – M.U., L.O.I., D.U.; Critical Review – M.U., L.O.I., S.O., D.P.O., O.Y.O., B.U.T., D.U.

Declaration of Interests: The authors have no conflict of interest to declare.

Funding: The authors declared that this study has received no financial support.

REFERENCES

1. K. K. Pal, and K. S. Sudeep, "Preprocessing for image classification by convolutional neural networks," 2016 IEEE International Conference on Recent Trends in Electronics, Information & Communication Technology (RTEICT), IEEE Publications, pp. 1778–1781, 2016. [CrossRef]
2. Y. A. LeCun, L. Bottou, G. B. Orr, and K.R. Müller, "Efficient backprop," in *Neural Networks: Tricks of the Trade*, 2nd ed. Heidelberg, Berlin: Springer, 2012, pp. 9–48.
3. A. Ayanzadeh *et al.*, "Cell segmentation of 2d phase-contrast microscopy images with deep learning method," 2019 Medical Technologies Congress (TIPEKNO), pp. 1–4, 2019. [CrossRef]
4. Y. S. Erdem, Ö. Yalçın Özuysal, D. Pesen Okvur, B. Töreyn, and D. Ünay, "An image segmentation method for wound healing assay images," *Nat. Appl. Sci. J.*, vol. 4, no. 1, pp. 30–37, 2021. [CrossRef]
5. F. Zernike, "Phase contrast, a new method for the microscopic observation of transparent objects," *Physica*, vol. 9, no. 7, pp. 686–698, 1942. [CrossRef]
6. S. Landry, P. L. McGhee, R. J. Girardin, and W. J. Keeler, "Monitoring live cell viability: Comparative study of fluorescence, oblique incidence reflection and phase contrast microscopy imaging techniques," *Opt. Express*, vol. 12, no. 23, pp. 5754–5759, 2004. [CrossRef]
7. A. J. Hand, T. Sun, D. C. Barber, D. R. Hose, and S. MacNeil, "Automated tracking of migrating cells in phase-contrast video microscopy sequences using image registration," *J. Microsc.*, vol. 234, no. 1, pp. 62–79, 2009. [CrossRef]
8. N. Jaccard *et al.*, "Automated method for the rapid and precise estimation of adherent cell culture characteristics from phase contrast microscopy images," *Biotechnol. Bioeng.*, vol. 111, no. 3, pp. 504–517, 2014. [CrossRef]
9. F. Xing, Y. Xie, H. Su, F. Liu, and L. Yang, "Deep learning in microscopy image analysis: A survey," *IEEE Trans. Neural Netw. Learn. Syst.*, vol. 29, no. 10, pp. 4550–4568, 2017.
10. H.F. Tsai, J. Gajda, T. F. W. Sloan, A. Rares, and A. Q. Shen, "Usiigaci: Instance-aware cell tracking in stain-free phase contrast microscopy enabled by machine learning," *SoftwareX*, vol. 9, pp. 230–237, 2019. [CrossRef]
11. T. Maison, "Lestari, and A. Luthfi, Retinal Blood Vessel Segmentation Using Gaussian Filter," *J. Phys. Conf. S.*, vol. 1376, no. 1, pp. 012–023, Nov 2019.
12. C. Li, Z. Chen, B. Sheng, P. Li, and G. He, "Video flickering removal using temporal reconstruction optimization," *Multimedia Tool. Appl.*, vol. 79, no. 7–8, pp. 4661–4679, 2020. [CrossRef]
13. S. Leger, S. Löck, V. Hietschold, R. Haase, H. J. Böhme, and N. Abolmaali, "Physical correction model for automatic correction of intensity non-uniformity in magnetic resonance imaging," *Phys. Imaging Radiat. Oncol.*, vol. 4, pp. 32–38, 2017. [CrossRef]
14. U. Vovk, F. Pernus, and B. Likar, "A review of methods for correction of intensity inhomogeneity in MRI," *IEEE Trans. Med. Imaging*, vol. 26, no. 3, pp. 405–421, 2007. [CrossRef]
15. B. Belaroussi, J. Milles, S. Carme, Y. M. Zhu, and H. Benoit-Cattin, "Intensity non-uniformity correction in MRI: Existing methods and their validation," *Med. Image Anal.*, vol. 10, no. 2, pp. 234–246, 2006. [CrossRef]
16. Z. Hou, "A review on MR image intensity inhomogeneity correction," *Int. J. Biomed. Imaging*, vol. 2006, pp. 49515, 2006. [CrossRef]
17. G. Xiao, M. Brady, J. A. Noble, and Y. Zhang, "Segmentation of ultrasound B-mode images with intensity inhomogeneity correction," *IEEE Trans. Med. Imaging*, vol. 21, no. 1, pp. 48–57, 2002. [CrossRef]
18. Y. Tendero, S. Landeau, and J. Gilles, "Non-uniformity correction of infrared images by midway equalization," *Image Process. On Line*, vol. 2, pp. 134–146, 2012. [CrossRef]
19. "Blank frame distortion's example data." [Online]. Available: <https://shorturl.at/ixlXZ>. [Accessed: 20.05.2023].
20. "Intensity variation distortion's example data." [Online]. Available: <https://shorturl.at/ehuBN>. [Accessed: 20.05.2023].
21. "Cell tracking challenge 2D time dataset." [Online], Available: 2D+Time Datasets – Cell Tracking Challenge [Accessed: 20.05.2023].
22. V. Ulman *et al.*, "An objective comparison of cell-tracking algorithms," *Nat. Methods*, vol. 14, no. 12, pp. 1141–1152, 2017. [CrossRef]
23. T. A. Ulrich, E. M. De Juan Pardo, and S. Kumar, "The mechanical rigidity of the extracellular matrix regulates the structure, motility, and proliferation of glioma cells," *Cancer Res.*, vol. 69, no. 10, pp. 4167–4174, 2009. [CrossRef]
24. "ImageJ software", [Online]. ImageJ. Available: <https://imagej.nih.gov/ij/> <https://imagej.nih.gov/ij/>. [Accessed: 20.05.2023].
25. "Half-normal distribution," [Online], Wikipedia, 2022. Available: https://en.wikipedia.org/wiki/Half-normal_distribution. [Accessed: 20.05.2023].



Mahmut Ucar received the B.S. degree in Electronics and Communication Engineering from Izmir Institute of Technology, Izmir, Turkey (2019). In 2019, he started M.S. studies at Biomedical Technologies Department of Ege University, Izmir, Turkey. Main focus area was image processing on thermal mammography matrices. At 2020, he started a new M.S. study in Electronics Engineering Department of Izmir Democracy University, Izmir, Turkey. Main focus area is building new conventional image processing methods for PCM images.



Leonardo Obinna IHEME received his Ph.D. in Electrical Electronics Engineering from Bahçeşehir University in 2018. He has extensive experience in the industry, utilizing artificial intelligence to solve computer vision problems for various companies. As an academic, his research focus includes medical imaging, computer vision, and AI, with publications in esteemed venues. Prior to his current position as a Senior Data Scientist at EPAM Systems, Dr. IHEME held roles such as Senior Research Fellow at the Mayo Clinic in Rochester, Senior AI Specialist at ViraSoft Inc. in Istanbul, and Research Engineer at AdresGezgini Inc. in Izmir.



Sevgi Onal has recently completed her MacDiarmid Institute sponsored PhD program in the Department of Electrical & Computer Engineering at University of Canterbury, New Zealand in 2022. Her Ph.D. research focuses on flexible micro-devices for characterization of the role of bionanomechanics in cancer. She received the M.Sc. degree in Biotechnology and Bioengineering Graduate Program of the Izmir Institute of Technology, Turkey, in 2017. Her Masters thesis examined the interaction mechanisms of cancer cells and macrophages on the EGF-EGFR axis by testing the hypotheses of chemotaxis, haptotaxis, or direct contact in a multidisciplinary approach, including microfluidics-based cell-on-a-chip technology. Her research interests include microfabrication, microfluidics, mechanobiology, 3D printing, microscopy, and live cell imaging.



Ozden Yalcin Ozuysal, received her M.Sc. in Molecular Biology and Genetics in 2004 from Bilkent University in Türkiye, and her Ph.D. in Life Sciences in 2009 from University of Lausanne in Switzerland. After working as post-doctoral research fellow in Ecole Polytechnique Federale de Lausanne in Switzerland, in 2010 she joined Molecular Biology and Genetics department in Izmir Institute of Technology (IZTECH) in Türkiye. She is working on molecular biology of cancer, specifically focusing on signaling pathways in cancer cell invasion and metastasis.



Devrim Pesen Okvur received her Ph.D. degree in Cellular and Molecular Physiology from the Johns Hopkins University in 2005. After postdoctoral studies at the Karolinska Institute, Royal Institute of Technology and Albert Einstein College of Medicine, she joined the faculty of Izmir Institute of Technology in 2010. Her research focuses on the design and fabrication of organ-on-chips that mimic the cellular microenvironment in addition to biophysical and micro-environmental control of the metastatic process in breast cancer.



Behcet Ugur Toreyin received the B.S. degree from the Middle East Technical University, Ankara, Turkey, in 2001 and the M.S. and Ph.D. degrees from Bilkent University, Ankara, in 2003 and 2009, respectively, all in electrical and electronics engineering. He is now a Full Professor with the Informatics Institute at Istanbul Technical University. His research interests broadly lie in signal processing and pattern recognition with applications to image/video analysis and communication systems. His research is focused on developing algorithms to analyze and compress signals from a multitude of sensors such as visible/infra-red/hyperspectral cameras, microphones, passive infra-red sensors, vibration sensors, and spectrum sensors for wireless communications: <http://spacing.itu.edu.tr>.



Devrim Unay received the B.S. degree in electrical and electronics engineering and the M.S. degree in biomedical engineering from Bogazici University, Turkey, and the Ph.D. degree in applied sciences from the Faculte Polytechnique de Mons, Belgium. He was a Senior Scientist and a Marie Curie Fellow with the Video Processing and Analysis Group, Philips Research Eindhoven, The Netherlands, a Visiting Researcher with the VPA Laboratory, Faculty of Engineering and Natural Sciences, Sabanci University, Istanbul, Turkey, and a Faculty Member with Biomedical Engineering Department, Faculty of Engineering and Natural Sciences, Bahcesehir University, Istanbul. He is currently a Faculty Member at the Electrical-Electronics Engineering Department of Izmir Democracy University, Turkey. His research interests include biomedical image analysis, computer vision and pattern recognition, content-based information retrieval, and machine/deep learning.